Amino Acids (2014) 46:1867–1883
DOI 10.1007/s00726-014-1737-8

ORIGINAL ARTICLE

Effect of side chain length on intrahelical interactions between carboxylate- and guanidinium-containing amino acids

Hsiou-Ting Kuo · Po-An Yang · Wei-Ren Wang · Hao-Chun Hsu · Cheng-Hsun Wu · Yu-Te Ting · Ming-Huei Weng · Li-Hung Kuo · Richard P. Cheng

Received: 15 January 2014 / Accepted: 21 March 2014 / Published online: 18 April 2014

Abstract The charge-containing hydrophilic functionalities of encoded charged amino acids are linked to the backbone via different numbers of hydrophobic methylenes, despite the apparent electrostatic nature of protein ion pairing interactions. To investigate the effect of side chain length of guanidinium- and carboxylate-containing residues on ion pairing interactions, α-helical peptides containing Zbb–Xaa $(i, i + 3)$, $(i, i + 4)$ and $(i, i + 5)$ (Zbb = carboxylate-containing residues Aad, Glu, Asp in decreasing length; Xaa = guanidinium residues Agh, Arg, Agb, Agp in decreasing length) sequence patterns were studied by circular dichroism spectroscopy (CD). The helicity of Aad- and Glu-containing peptides was similar and mostly pH independent, whereas the helicity of Asp-containing peptides was mostly pH dependent. Furthermore, the Arg-containing peptides consistently exhibited higher helicity compared to the corresponding Agp-, Agb-, and Agh-containing peptides. Side chain conformational analysis by molecular mechanics calculations showed that the Zbb–Xaa $(i, i + 3)$ and $(i, i + 4)$ interactions mainly involved the χ_1 dihedral combinations $(g+, g+)$ and $(g-, g+)$, respectively. These low energy conformations were also observed in intrahelical Asp–Arg and Glu–Arg salt bridges of natural proteins. Accordingly, Asp and Glu provides variation in helix characteristics associated with Arg, but Aad does not provide features beyond those already delivered by Glu. Importantly, nature may have chosen the side chain length of Arg to support helical conformations through inherent high helix propensity coupled with stabilizing intrahelical ion pairing interactions with the carboxylate-containing residues.

Keywords Carboxylate · Guanidinium · Side chain length · α-Helix · Ion pairing interaction

Abbreviations

Aad	(*S*)-aminoadipate
Agb	(*S*)-2-amino-4-guanidinobutyric acid
Agh	(*S*)-2-amino-6-guanidinohexanoic acid
Agp	(*S*)-2-amino-3-guanidinopropionic acid
Ala	Alanine
Arg	Arginine
Asp	Aspartate
CD	Circular dichroism spectroscopy
Fmoc	N^{α}-fluorenylmethyloxycarbonyl
Glu	Glutamate
Lys	Lysine
MALDI-TOF	Matrix-assisted laser desorption ionization time-of-flight
Tyr	Tyrosine

Introduction

Proteins are biological macromolecules that perform the biochemical function for many vital processes in living organisms. In general, a well-defined three-dimensional protein structure is required for performing these biochemical functions (Creighton 1993; Fersht 1999). Amino

Electronic supplementary material The online version of this article (doi:10.1007/s00726-014-1737-8) contains supplementary material, which is available to authorized users.

H.-T. Kuo · P.-A. Yang · W.-R. Wang · H.-C. Hsu · C.-H. Wu · Y.-T. Ting · M.-H. Weng · L.-H. Kuo · R. P. Cheng (✉)
Department of Chemistry, National Taiwan University, Taipei 10617, Taiwan
e-mail: rpcheng@ntu.edu.tw

acids are the basic chemical building blocks for proteins. The encoded amino acids are linked by amide bonds in a particular order based on the genetic code to give the protein polypeptide chain. The polypeptide chain forms local secondary structures such as α-helices and β-sheets (Anfinsen 1973; Rose et al. 2006; Dill et al. 2008). These protein secondary structures are assembled into tertiary protein structures with well-defined three-dimensional conformations (Baldwin and Rose 1999a, b). This assembly process is driven by non-covalent forces including electrostatics, hydrogen bonds, hydrophobics, and van der Waals interactions (Pace et al. 1996; Dill 1990; Dill et al. 2008; Makhatadze and Privalov 1995).

Electrostatic ion pairing interactions are prevalent in many biological inter- and intramolecular interactions (Jiang et al. 2003), and especially in proteins (Barlow and Thornton 1983). Charged residues are distributed throughout the protein structure, playing critical roles in protein folding by providing attractive and repulsive electrostatic interactions. The attractive electrostatic interactions between oppositely charged amino acids have been shown to be important for protein structure stability (Dill 1990; Makhatadze and Privalov 1995). Interestingly, thermophilic proteins exhibit more stabilizing electrostatic profiles compared to mesophilic proteins (Pace 2000; Elcock 1998; Yip et al. 1998; Malakauskas and Mayo 1998; Xiao and Honig 1999; Karshikoff and Ladenstein 2001; Kumar and Nussinov 2002; Dominy et al. 2004; Thomas and Elcock 2004; Robinson-Rechavi et al. 2006; Su et al. 2010), suggesting that attractive electrostatic interactions can enhance the stability of the three-dimensional structure (Klingler and Brutlag 1994; Barlow and Thornton 1983; Maxfield and Scheraga 1975).

The encoded charged amino acids arginine (Arg), lysine (Lys), glutamate (Glu), and aspartate (Asp) participate in protein electrostatics interactions. Interestingly, these four amino acids have different side chain lengths. The positively and negatively charged functionalities contribute to the electrostatic component of ion pairing interactions, leaving the role of the linking hydrophobic methylenes unclear. Although arginine and lysine are both positively charged residues with side chain pK_a values >10, Arg is different from Lys in bearing a guanidinium group to carry the positive charge instead of an ammonium group. This creates a more diffuse positive charge, higher hydrogen bonding capacity, and different overall geometry for Arg compared to Lys. The difference between the two residues is reflected in the secondary structure propensities (Padmanabhan et al. 1996; Cheng et al. 2012b; Kuo et al. 2013). Helix propensity decreases upon shortening the Lys side chain length (Padmanabhan et al. 1996). In contrast, either shortening or lengthening the Arg side chain length decreases helix propensity (Cheng et al. 2012b). As for sheet formation energetics, shortening the Lys side chain disfavors β-strand formation (Kuo et al. 2013), whereas lengthening the Arg side chain favors β-strand formation (Kuo et al. 2013).

A survey on protein salt bridges showed high statistical propensity for both intrahelical Asp–Arg and Glu–Arg (i, $i + 3$) salt bridges (Donald et al. 2011), but only for intrahelical Glu–Arg (i, $i + 4$) salt bridges (Donald et al. 2011), implying different effects for different spacings on intrahelical salt bridges involving Arg. However, high statistical propensity was observed for only Glu–Lys (i, $i + 3$) and Asp–Lys (i, $i + 4$) salt bridges (Donald et al. 2011). These results suggest that Arg and Lys are applied differently in natural protein structures. The effect of the Lys side chain length on intrahelical ion pairing interactions between carboxylate- and ammonium-bearing residues has been studied in quite some detail (Scholtz et al. 1993; Cheng et al. 2007, 2012a). Furthermore, limited experimental studies on intrahelical ion pairing interactions involving Arg have also provided some information on the difference between Glu and Asp (Huyghues-Despointes et al. 1993b). Higher helicity for Glu-containing peptides compared to Asp-containing peptides was observed for peptides with potential intrahelical Glu/Asp–Arg interactions involving (i, $i + 3$) and (i, $i + 4$) spacings (Huyghues-Despointes et al. 1993b). However, how the side chain length of the guanidinium-bearing Arg affects intrahelical ion pairing interactions remains unknown. Herein, a systematic comprehensive study on the effect of side chain length on intrahelical interactions between guanidinium- and carboxylate-containing residues was investigated by circular dichroism spectroscopy coupled with modified Lifson–Roig theory (Lifson and Roig 1961) and the nesting block method (Chakrabartty et al. 1994; Doig and Baldwin 1995), conformational analysis using molecular mechanics calculations, and a survey of a non-redundant protein structure database.

Results

Peptide design and synthesis

The sequences were designed based on monomeric α-helical peptides with intrahelical Glu–Lys (i, $i + 3$) or (i, $i + 4$) interactions (Fig. 1) (Marqusee and Baldwin 1987; Cheng et al. 2007, 2012a). The guanidinium-bearing positively charged residue Xaa was systematically shortened from (*S*)-2-amino-6-guanidinohexanoic acid (Agh, 4 methylenes) to Arg (3 methylenes), to (*S*)-2-amino-4-guanidinobutyric acid (Agb, 2 methylenes), and to (*S*)-2-amino-3-guanidinopropionic acid (Agp, 1 methylene) (Fig. 1). Similarly, the negatively charged residues Zbb

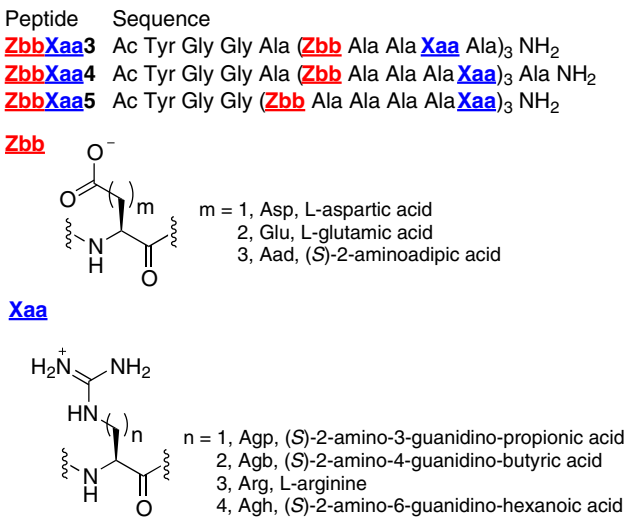

Fig. 1 Sequences for the ZbbXaa3, ZbbXaa4, and ZbbXaa5 peptides. The underlined generic 3-letter codes Zbb and Xaa represent the negatively and positively charged residues, respectively

was systematically lengthened from Asp (one methylene) to Glu (two methylenes) to (*S*)-2-aminoadipic acid (Aad, three methylenes) (Fig. 1). The peptides were named according to the three-letter code of the negatively and positively charged residues and the spacing between the charged residues. Since an ideal α-helix would have 3.6 residues per turn (Pauling et al. 1951), residues spaced 3 and 4 residues apart could potentially interact in the ZbbXaa3 and ZbbXaa4 peptides, respectively (Fig. 1). The oppositely charged amino acids were spaced 5 residues apart in the ZbbXaa5 peptides (Fig. 1), and should not interact based on the α-helix geometry, results by other researchers (Smith and Scholtz 1998; Pace and Scholtz 1998), and our previous studies (Cheng et al. 2007, 2012a). The overall distribution of the charged residues was designed to stabilize the α-helix macrodipole by placing the negatively charged residue with a carboxylate group (Zbb) closer to the N-terminus and the positively charged residue with a guanidinium group (Xaa) closer to the C-terminus (Marqusee and Baldwin 1987; Cheng et al. 2007, 2012a). Tyrosine was incorporated to facilitate concentration determination by UV–vis using the Edelhoch method (Edelhoch 1967; Pace et al. 1995), and the two intervening Gly residues were included to minimize interference with the CD signal by the Tyr chromophore (Chakrabartty et al. 1994).

The peptides were synthesized by solid-phase peptide synthesis using Fmoc-based chemistry (Fields and Noble 1990; Atherton et al. 1978). The Agh-containing peptides were synthesized using Fmoc-Agh(Boc)$_2$-OH by standard coupling protocols (Cheng et al. 2012b). The Agb- and Agp-containing peptides were synthesized by solid phase guanidinylation (Cheng et al. 2012b), because Agb- and Agp-containing peptides could not be directly synthesized using Fmoc-Agb(Boc)$_2$-NH$_2$ and Fmoc-Agp(Boc)$_2$-NH$_2$ (Cheng et al. 2012b), respectively. All peptides were purified by reverse-phase high-performance liquid chromatography to greater than 98.5 % purity and confirmed by MALDI-TOF mass spectrometry. The peptide stock concentrations were determined by UV–vis as described by Edelhoch (Edelhoch 1967; Pace et al. 1995).

Circular dichroism spectroscopy

The circular dichroism (CD) spectra of the peptides were acquired at pH 7 in the absence of sodium chloride (Fig. 1; Table S1). At pH 7, the carboxylate- and guanidinium-containing residues are negatively charged and positively charged, respectively, allowing potential intrahelical ion pairing interactions. The magnitude of the CD signal at 222 nm reflects the α-helical content of a peptide (Chang et al. 1978). Analogous peptides did not aggregate in aqueous solution (Marqusee and Baldwin 1987; Cheng et al. 2007, 2012a; Huyghues-Despointes et al. 1993b), therefore, the peptides in this study should not aggregate either. Furthermore, the CD spectra of the peptides were independent of peptide concentration (50–100 μM), suggesting no aggregation in this concentration range. As such, the CD spectra should represent the intramolecular interactions with minimal interference from intermolecular interactions.

The helical content of ZbbXaa5 peptides for a given negatively charged residue Zbb followed the general trend ZbbAgh5 ≤ ZbbArg5 ≥ ZbbAgb5 > ZbbAgp5 (Fig. 2c, f, i; Table S1), consistent with the helix propensity trend Agh < Arg > Agb > Agp (Cheng et al. 2012b). In general, the helical content of the ZbbXaa5 peptides increased with increasing negatively charged residue Zbb side chain length for a given positively charged residue Xaa, consistent with the helix propensity trend of the negatively charged residues (Huyghues-Despointes et al. 1993a; Scholtz et al. 1993; Chakrabartty et al. 1994; Doig and Baldwin 1995; Cheng et al. 2012a). This appears to be consistent with the lack of Zbb–Xaa (i, $i + 5$) interactions and the helix geometry. Nonetheless, the helical content of the Arg-containing peptides was higher compared to that of the corresponding peptides with other Arg analogs.

The helical content of ZbbXaa4 peptides for a given negatively charged residue Zbb followed the general trend ZbbAgh4 ≤ ZbbArg4 ≥ ZbbAgb4 > ZbbAgp4 (Fig. 2b, e, h; Table S1), consistent with the helix propensity trend Agh < Arg > Agb > Agp (Cheng et al. 2012b). Interestingly, the Arg side chain could be lengthened or shortened by one methylene with only minimal effect on the helical content of the AadXaa4 peptides, suggesting significant Aad–Xaa (i, $i + 4$) interaction involving Arg, Agh, and

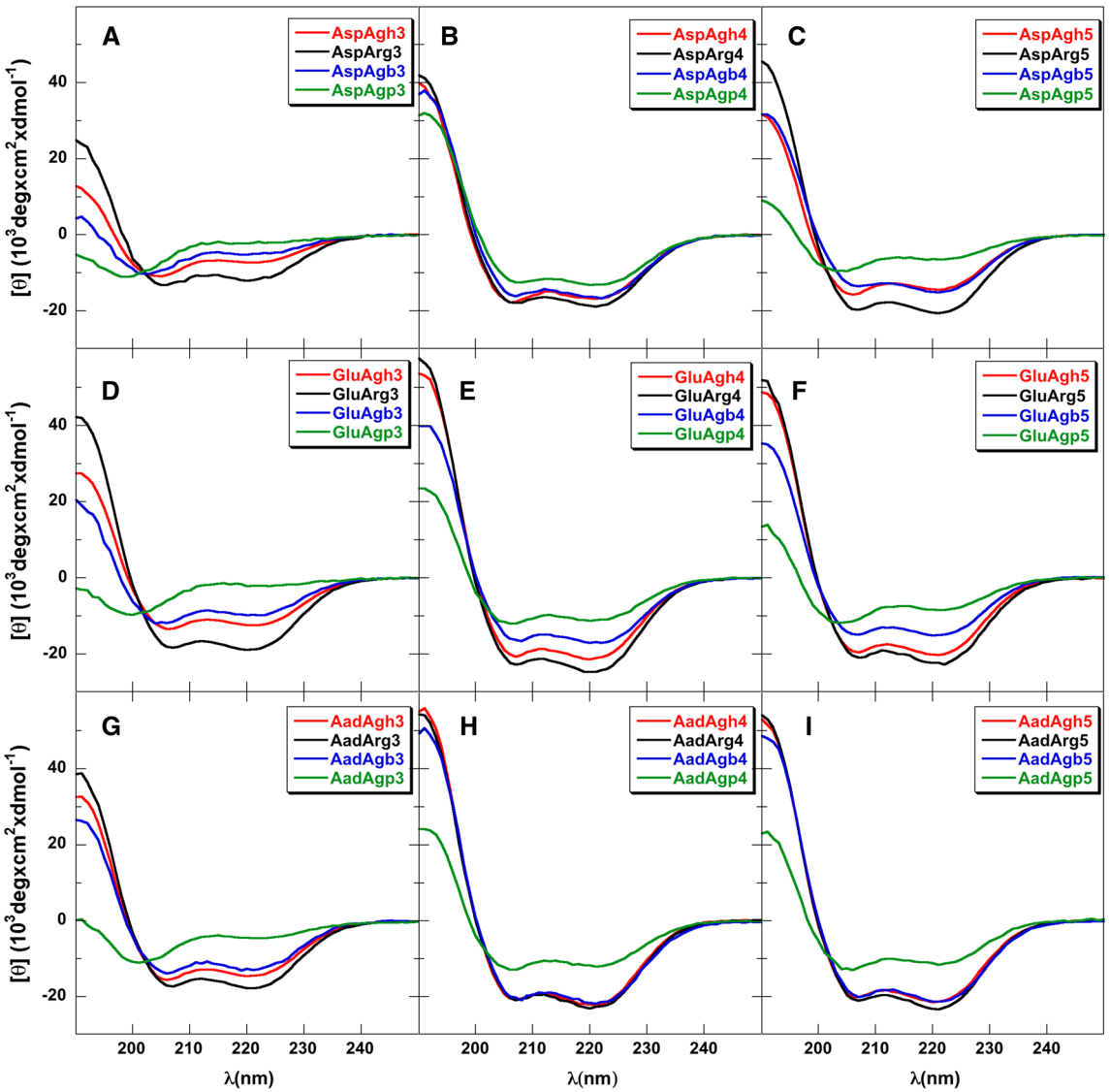

Fig. 2 Circular dichroism spectra of the peptides at pH 7 (273 K) in 1 mM of phosphate, borate, and citrate buffer in mean residue ellipticity (**a** AspAgh3, AspArg3, AspAgb3, AspAgp3; **b** AspAgh4, AspArg4, AspAgb4, AspAgp4; **c** AspAgh5, AspArg5, AspAgb5, AspAgp5; **d** GluAgh3, GluArg3, GluAgb3, GluAgp3; **e** GluAgh4, GluArg4, GluAgb4, GluAgp4; **f** GluAgh5, GluArg5, GluAgb5, GluAgp5; **g** AadAgh3, AadArg3, AadAgb3, AadAgp3; **h** AadAgh4, AadArg4, AadAgb4, AadAgp4; **i** AadAgh5, AadArg5, AadAgb5, AadAgp5)

Agb. For the Agb- and Agh-containing ZbbXaa4 peptides, the helical content increased with increasing negatively charged residue Zbb side chain length, consistent with the helix propensity trend of the negatively charged residues (Huyghues-Despointes et al. 1993a; Scholtz et al. 1993; Chakrabartty et al. 1994; Doig and Baldwin 1995; Cheng et al. 2012a). However, for the Agp-containing peptides, the helical content followed the trend AspAgp4 > AadAgp4 > GluAgp4, suggesting the presence of Zbb–Agp (i, $i + 4$) interactions. For the Arg-containing peptides, the helical content followed the trend GluArg4 > AadArg4 > AspArg4, also suggesting the presence of Zbb–Arg (i, $i + 4$) interactions. Importantly, the Arg-containing peptides consistently exhibited the most helical content for any given negatively charged residue in the ZbbXaa4 peptides compared to the corresponding peptides with the other Arg analogs.

The helical content of ZbbXaa3 peptides followed the trend ZbbAgh3 < ZbbArg3 > ZbbAgb3 > ZbbAgp3 (Fig. 2a, d, g; Table S1), consistent with the helix propensity for the positively charged residues (Cheng et al. 2012b). In general, the helical content of the ZbbXaa3 peptides increased with increasing negatively charged Zbb side chain length for a given positively charged residue except for Arg. The higher than expected helical content for GluArg3 suggested the presence of helix stabilizing

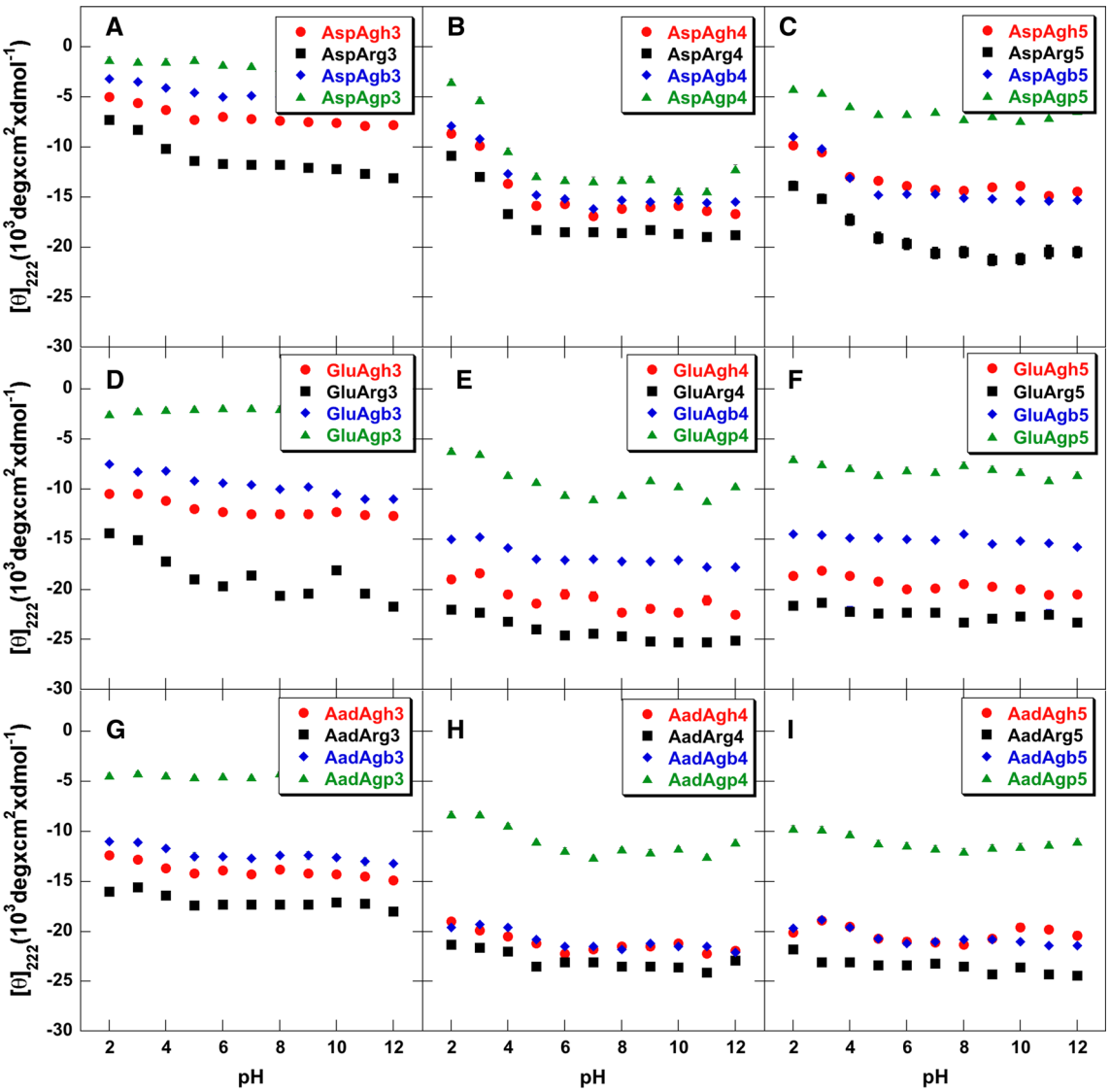

Fig. 3 Circular dichroism signal at 222 nm of the peptides at pH 2–12 (273 K) in 1 mM of phosphate, borate, and citrate buffer in mean residue ellipticity (**a** AspAgh3, AspArg3, AspAgb3, AspAgp3; **b** AspAgh4, AspArg4, AspAgb4, AspAgp4; **c** AspAgh5, AspArg5, AspAgb5, AspAgp5; **d** GluAgh3, GluArg3, GluAgb3, GluAgp3; **e** GluAgh4, GluArg4, GluAgb4, GluAgp4; **f** GluAgh5, GluArg5, GluAgb5, GluAgp5; **g** AadAgh3, AadArg3, AadAgb3, AadAgp3; **h** AadAgh4, AadArg4, AadAgb4, AadAgp4; **i** AadAgh5, AadArg5, AadAgb5, AadAgp5)

Glu–Arg (i, $i + 3$) interactions. For a given negatively charged residue Zbb, the helical content of the Arg-containing peptides consistently exhibited the highest helical content for the ZbbXaa3 peptides compared to peptides containing other Arg analogs.

The CD signal at 222 nm for all peptides was measured between pH 2 and 12 to provide insight into the nature of the Zbb–Xaa intrahelical interactions (Fig. 3). However, the data at high pH could not be interpreted without ambiguity because the pK_a of the Tyr (tyrosine) phenol side chain is near 10, and aromatic groups can contribute to the CD signal (Chakrabartty et al. 1993). Furthermore, the helix dipole can perturb the pK_a by 1.6 pH units (Sali et al. 1988; Johnsson et al. 1993), thus only data between pH 2 and 7 will be discussed. Changing the pH from 7 to 2 should protonate and neutralize the carboxylate side chain of the negatively charged residue Zbb$^-$. The helical content of same peptide at the two different pH values were considered to be significantly different if the CD signal of the less helical signal was <70 % of the more helical signal, and the P value for comparing the two CD signals was $<10^{-5}$. The helicity of Glu- and Aad-containing peptides (except for GluAgp4 and AadAgp4) did not change significantly upon lowering the pH from 7 to 2 (Fig. 3; Table S1). In contrast, the helicity of most Asp-containing peptides was significantly attenuated upon changing the pH from 7 to 2 (Fig. 3; Table S1).

The AspXaa5 peptides exhibited significantly less helical content at pH 2 compared to pH 7 (Fig. 3c; Table S1), whereas the GluXaa5 and AadXaa5 peptides exhibited similar helical content at pH 2 and 7 (Fig. 3c, f, i; Table S1). For AspXaa4 peptides, the helical content decreased significantly upon lowering the pH from 7 to 2 (Fig. 3b; Table S1). In contrast, there was minimal change in the CD signal for the GluXaa4 and AadXaa4 peptides (Fig. 3e, h; Table S1), except for peptides GluAgp4 and AadAgp4. For ZbbXaa3 peptides, only the Asp-containing peptides exhibited significant helical content attenuation upon lowering the pH from 7 to 2 (Fig. 3a, d, g; Table S1).

The CD spectra of the ZbbXaa3, ZbbXaa4, and ZbbXaa5 peptides at pH 2 were acquired to probe the intrahelical Zbb–Xaa interactions involving neutral Zbb^0 side chains (Fig. S1; Table S1). The helical content trends of the ZbbXaa5, ZbbXaa4, and ZbbXaa3 peptides were similar at pH 2 and pH 7 (Fig. S1; Table S1). The Asp-containing peptides consistently exhibited less helicity at pH 2 compared to the corresponding Glu- and Aad-containing peptides (Fig. S1; Table S1). Furthermore, the helical content of the Arg-containing peptides at pH 2 were higher compared to the corresponding peptides with other positively charged residues.

Intrahelical Zbb–Xaa interaction energetics at pH 7 and pH 2

The side chain–side chain interaction energy at pH 7 ($\Delta G_{pH\ 7}$) and 2 ($\Delta G_{pH\ 2}$) was derived from the CD data using the modified nesting block method (Tables 1, 2, S2) (Scholtz et al. 1993; Robert 1990; Cheng et al. 2007, 2012a), to determine the effect of side chain length on intrahelical side chain interactions. At first glance, the helical content and the interaction energies may appear to contradict one another. This apparent discrepancy is because the helical content is determined by multiple factors including the helix propensity of the constituting amino acids, the sequence, the interaction between the charged residues and the helix macrodipole, and the intrahelical side chain interactions (Cheng et al. 2007, 2012a; Scholtz et al. 1993).

No significant Glu^-/Aad^-–Xaa (i, $i + 5$) interaction energy was observed for the ZbbXaa5 peptides (Table S2), consistent with the α-helical structure. However, AspXaa5 peptides appeared to exhibit intrahelical ion pairing interaction energy at pH 7 (Tables 2, S2), following the trend Agp > Agb > Arg > Agh. For the ZbbXaa3 peptides, stabilizing Zbb^-–Xaa (i, $i + 3$) interactions were observed only for the AspXaa3 peptides at pH 7 (Tables 2, S2), following the trend Arg > Agh ~ Agb. No stabilizing Zbb^-–Xaa (i, $i + 3$) interaction energy was observed upon lengthening Asp to Glu or Aad, or when the positively charged residue contained only one methylene (Agp).

Helix stabilizing Zbb^-–Xaa (i, $i + 4$) interactions were present at pH 7 for most residue combinations except for Asp–Agp, Glu–Agp, Aad–Agh, and Aad–Arg (Tables 1, S2). The magnitude of the Asp^-–Xaa (i, $i + 4$) interaction energy followed the trend Agb > Arg ≥ Agh. Apparently, the shorter the positively charged residue side chain, the more stabilizing the ion pairing interaction. However, the positively charged residue Agp with the shortest side chain

Table 1 Energetics[a] of Zbb–Xaa (i, $i + 4$) intrahelical interactions at pH 7 and 2

Residue i	Residue $i + 4$	$\Delta G_{pH\ 7}$ (kcal mol^{-1})	$\Delta G_{pH\ 2}$ (kcal mol^{-1})	$\Delta\Delta G$[b] (kcal mol^{-1})
Asp	Agh	−0.239 ± 0.012	ND[c]	−0.239 ± 0.012
Asp	Arg	−0.259 ± 0.006	−0.108 ± 0.005	−0.151 ± 0.008
Asp	Agb	−0.520 ± 0.009	−0.270 ± 0.021	−0.250 ± 0.023
Asp	Agp	ND[c]	ND[c]	
Glu	Agh	−0.183 ± 0.017	−0.104 ± 0.014	−0.079 ± 0.022
Glu	Arg	−0.176 ± 0.011	−0.062 ± 0.010	−0.114 ± 0.015
Glu	Agb	−0.188 ± 0.009	−0.105 ± 0.009	−0.083 ± 0.013
Glu	Agp	ND[c]	ND[c]	
Aad	Agh	ND[c]	ND[c]	
Aad	Arg	ND[c]	ND[c]	
Aad	Agb	−0.083 ± 0.014	−0.118 ± 0.010	0.035 ± 0.017
Aad	Agp	−0.167 ± 0.011	ND[c]	−0.167 ± 0.011

[a] The energetic values $\Delta G_{pH\ 7}$ and $\Delta G_{pH\ 2}$ were derived from the experimental CD data based on the nesting block method (Scholtz et al. 1993; Robert 1990; Cheng et al. 2007, 2012a)

[b] $\Delta\Delta G = \Delta G_{pH\ 7} - \Delta G_{pH\ 2}$. The difference in side chain–side chain interaction energy at pH 7 and 2, which reflects the contribution of electrostatics in the Zbb–Xaa (i, $i + 4$) interaction

[c] The experimental results are within error of the calculated predicted values without any side chain–side chain interaction

Table 2 Energetics[a] of Asp–Xaa (i, $i + 3$) and (i, $i + 5$) intrahelical interactions at pH 7 and 2

Residue i	Residue $i + n$	n	$\Delta G_{pH\ 7}$ (kcal mol^{-1})	$\Delta G_{pH\ 2}$ (kcal mol^{-1})	$\Delta\Delta G$[b] (kcal mol^{-1})
Asp	Agh	3	−0.101 ± 0.007	ND[c]	−0.101 ± 0.007
Asp	Arg	3	−0.150 ± 0.012	ND[c]	−0.150 ± 0.012
Asp	Agb	3	−0.100 ± 0.022	ND[c]	−0.100 ± 0.022
Asp	Agb	3	ND[c]	ND[c]	ND[c]
Asp	Agh	5	−0.089 ± 0.007	ND[c]	−0.089 ± 0.007
Asp	Arg	5	−0.176 ± 0.018	−0.060 ± 0.018	−0.116 ± 0.025
Asp	Agb	5	−0.249 ± 0.007	−0.088 ± 0.012	−0.161 ± 0.014
Asp	Agp	5	−0.338 ± 0.019	ND[c]	−0.338 ± 0.019

[a] The energetic values $\Delta G_{pH\ 7}$ and $\Delta G_{pH\ 2}$ were derived from the experimental CD data based on the nesting block method (Scholtz et al. 1993; Robert 1990; Cheng et al. 2007, 2012a)

[b] $\Delta\Delta G = \Delta G_{pH\ 7} - \Delta G_{pH\ 2}$. The difference in side chain–side chain interaction energy at pH 7 and 2 reflects the contribution of electrostatics in the Zbb–Xaa (i, $i + n$) interaction

[c] The experimental results are within error of the calculated predicted values without any side chain–side chain interaction

contributed no stabilizing interaction energy towards helix stability. Similarly, there was no stabilizing interaction energy for the Glu^-–Agp (i, $i + 4$) pair. Perhaps the lack of helix stabilizing intrahelical Asp^-/Glu^-–Agp (i, $i + 4$) interactions is because Agp is too short to reach the shorter ion pairing partners Asp^- and Glu^-, but can reach the longer ion pairing partner Aad^-. The helix stabilizing energetics for the Glu^-–Agb/Arg/Agh (i, $i + 4$) interactions at pH 7 was similar. Interestingly, the Aad^-–Arg/Agh (i, $i + 4$) interactions did not stabilize the helix, whereas the Aad^-–Agp (i, $i + 4$) interaction was more stabilizing compared to the Aad^-–Agb (i, $i + 4$) interaction (Tables 1, S2). In general, the Zbb^-–Xaa (i, $i + 4$) interactions became more energetically stabilizing as the negatively charged residue Zbb side chain length decreased. Furthermore, oppositely charged residues with matching lengths (such as Aad–Arg/Agh, Asp/Glu–Agp) resulted in the lack of apparent stabilizing intrahelical interaction.

Changing the pH from 7 to 2 would protonate and neutralize the negatively charged Zbb^- to Zbb^0 and disrupt the electrostatic interactions with Zbb^- (including Zbb^-–Xaa and Zbb^-–helix macrodipole interactions). Therefore, the Zbb^0–Xaa interaction at pH 2 should represent the non-electrostatic components of the Zbb^-–Xaa interaction, including hydrogen bonding (Marqusee and Baldwin 1987; Huyghues-Despointes et al. 1993b) and hydrophobics (Andrew et al. 2001; Cheng et al. 2007). Most ZbbXaa5 peptides (except for AspAgb5 and AspArg5) did not exhibit any significant Zbb^0–Xaa (i, $i + 5$) interaction at pH 2 (Tables 2, S2), consistent with the α-helical structure. Also, no Zbb^0–Xaa (i, $i + 3$) interactions were observed for the ZbbXaa3 peptides at pH 2 (Tables 2, S2).

Among the ZbbXaa4 peptides, only AspAgb4, AspArg4, GluAgb4, GluArg4, GluAgh4, and AadAgb4 exhibited Zbb^0–Xaa (i, $i + 4$) interactions at pH 2 (Tables 1, S2). None of the Agp-containing peptides exhibited any Zbb^0–Xaa (i, $i + 4$) interaction. In contrast, increasing the Agp side chain length by only one methylene to Agb provided stabilizing Zbb^0–Agb (i, $i + 4$) interactions (with Asp, Glu, and Aad). For ZbbArg4 peptides, only Asp^0–Arg (i, $i + 4$) and Glu^0–Arg (i, $i + 4$) interactions were stabilizing. Furthermore, the Zbb^0–Arg (i, $i + 4$) interactions were less stabilizing compared to the corresponding Zbb^0–Agb (i, $i + 4$) interactions (Tables 1, S2).

The helix stabilizing Zbb^-–Xaa (i, $i + 4$) interactions at pH 7 generally became more stabilizing as the negatively charged residue Zbb side chain length decreased. This result was counterintuitive, because if sufficient side chain length is required for reaching the ion pairing partner, then the shorter side chains should exhibit less stabilizing interaction energy compared to the longer side chains. To explore if the side chain length is for reaching the ion pairing partner and to provide conformational insight into the intrahelical side chain interactions, conformational analysis was performed by molecular mechanics calculations.

Conformational analysis of short model peptides

A detailed conformational analysis on short model peptides was performed by molecular mechanics calculations to gain further insight into the effect of side chain length on potential side chain interactions. Three series of model hexapeptides were investigated: MSZbbXaa3, MSZbbXaa4, and MSZbbXaa5 (Fig. 4). All model peptides included one potential side chain–side chain interaction between a negatively charged amino acid (Asp, Glu, or Aad) and a positively charged residue (Agh, Arg, Agb, or Agp) placed three, four, or five residues apart. For each side chain dihedral angle (or χ angle) involving sp^3

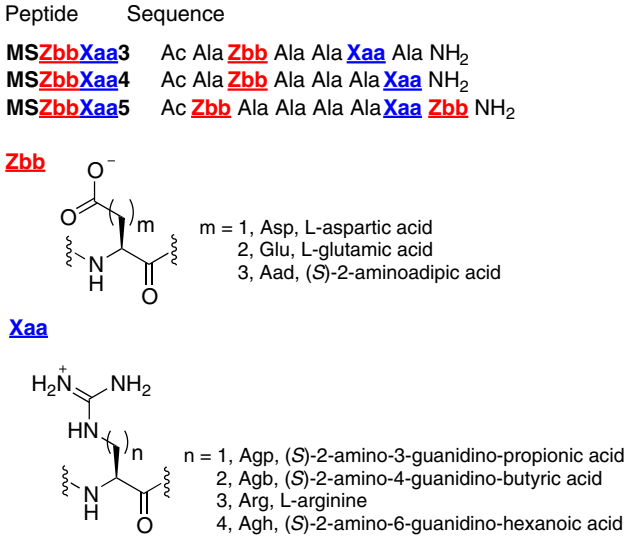

Fig. 4 Sequences of the short MSZbbXaa3, MSZbbXaa4, and MSZbbXaa5 model peptides for the conformational analysis by molecular mechanics calculations. The *underlined generic 3-letter codes* Zbb and Xaa represent the negatively and positively charged residues, respectively

carbons, three possible low energy staggered conformations were considered: gauche− (60°, *g*−), trans (180°, *t*), and gauche+ (300°, *g*+) (McGregor et al. 1987; Dunbrack and Karplus 1993). For the dihedral angle involving the sp^2 carboxylate carbon of the negatively charged amino acid, six conformations were considered: 0°, 30°, 60°, 90°, 120°, and 150°. For the dihedral angle involving the sp^2 nitrogen for guanidinium group of the positively charged amino acid, 12 conformations were considered: 0°, 30°, 60°, 90°, 120°, 150°, 180°, 210°, 240°, 270°, 300°, 330°. All possible χ angle combinations for the negatively charged residue Zbb and the positively charged residue Xaa were investigated. A combined total of 1,010,880 conformations were minimized.

The energy of the model peptides with the same positively charged residue and negatively charged residues (e.g., MSAspArg3, MSAspArg4, and MSAspArg5) could be compared, because the peptides were designed to have the same number of constituting atoms represented by the same force field parameters. The interactions between oppositely charged residues with different spacings were compared by evaluating the energy of the lowest energy conformers for the model peptides (Tables 3, S3). In general, the lowest energy conformers of the MSZbbXaa5 model peptides exhibited higher energy (less negative energy, i.e., less stable) compared to those of the corresponding MSZbbXaa4 and MSZbbXaa3 model peptides (Table S3), except for model peptide MSAspAgp5. Model peptide MSAspAgp5 was similar in energy compared to model peptide MSAspAgp3, most likely due to minimal side chain interactions in model peptide MSAspAgp3 (vide infra). The MSAspXaa4 and MSGluXaa4 model peptides were lower in energy (i.e., more stable) compared to the MSAspXaa3 and MSGluXaa3 model peptides (Tables 3, S3), respectively, suggesting that the Asp–Xaa and Glu–Xaa (Xaa = Agh, Arg, Agb, Agp) interactions should be energetically more favorable with (i, $i + 4$) spacing compared to (i, $i + 3$) spacing. This is consistent with the experimental data at pH 7 showing higher helical content and more stabilizing side chain interactions for the AspXaa4 and GluXaa4 peptides (Fig. 2; Tables S1, S2), and lower helical content and less stabilizing side chain interactions for the AspXaa3 and GluXaa3 peptides (Fig. 2; Tables S1, S2). In contrast, small energy differences were observed for MSAadXaa peptides with (i, $i + 4$) and (i, $i + 3$) spacings (Tables 3, S3), also consistent with the low or lack of experimentally derived interaction energy for Aad-containing peptides with either spacing (Table S2). Overall, these computational results are generally consistent with the CD results and experimentally derived interaction energies at pH 7 ($\Delta G_{\mathrm{pH\ 7}}$) (Fig. 2; Tables 1, 2, S1, S2).

Conformations within 4 kcal of the lowest energy conformer for each peptide were then examined (Tables 3, S3), because room temperature can provide up to 4 kcal mol^{-1} of thermal energy (Cheng et al. 2007, 2012a, b). In general, the number of conformations increased with increasing side chain length, consistent with higher side chain conformational entropy for longer side chains compared to shorter side chains. The weighed average energy (based on Boltzmann distribution) of the peptides followed the same trends as the lowest energy for each peptide (vide supra) (Table S3). Importantly, none of the MSZbbXaa5 model peptides exhibited intrahelical Zbb–Xaa salt bridges (Table S3), consistent with the α-helix geometry. In general, the MSGluXaa4 and MSAspXaa4 model peptides exhibited a higher percentage of conformations with intrahelical salt bridges compared to the corresponding MSGluXaa3 and MSAspXaa3 model peptides (Table 3, S3), respectively, consistent with the CD data at pH 7 (Fig. 2). However, the MSAadAgb4 and MSAadAgp4 model peptides exhibited a lower percentage of conformations with intrahelical salt bridges but many more low energy conformers compared to the corresponding MSAadAgb3 and MSAadAgp3 model peptides (Table 3, S3), respectively. The energy should reflect the enthalpic component for the peptide conformations, whereas the number of low energy conformers may be viewed as a crude estimate of the entropic component for the peptides. The combination of the two components suggests that Aad–Agb (i, $i + 4$) and Aad–Agp (i, $i + 4$) interactions may be more favorable compared to the corresponding Aad–Xaa (i, $i + 3$) (as derived experimentally) due to

Table 3 Summary of low energy conformations from conformational analysis of MSZbbXaaN peptides by molecular mechanics calculations

Peptide	Lowest energy conformer Energy (kcal)	Conformations within 4 kcal of the lowest energy conformer		
		No[a]	Salt bridge[b] (%)	Major conformations with salt bridge, number (Zbb χ_1, Xaa χ_1)[c]
MSAspAgh3	−156.8	23	91	20($g+$, $g+$), 1($g+$, t)
MSAspAgh4	−160.7	18	100	15($g-$, $g+$), 2($g+$, $g+$), 1($g-$, t)
MSAspArg3	−152.6	10	100	7($g+$, $g+$), 3($g+$, t)
MSAspArg4	−155.4	7	100	7($g-$, $g+$)
MSAspAgb3	−145.9	24	17	4($g+$, $g+$)
MSAspAgb4	−153.2	3	100	3($g-$, $g+$)
MSAspAgp3	−140.1	30	13	3(t, $g-$), 1($g+$, $g-$)
MSAspAgp4	−145.0	19	21	4(t, $g+$)
MSGluAgh3	−155.4	18	100	18($g+$, $g+$)
MSGluAgh4	−157.1	42	100	40($g-$, $g+$), 2($g+$, $g+$)
MSGluArg3	−149.5	19	89	12($g+$, $g+$), 3($g+$, t), 1(t, t), 1(t, $g+$)
MSGluArg4	−151.5	13	85	6($g-$, $g+$), 4($g-$, t), 1(t, $g+$)
MSGluAgb3	−145.9	24	25	5($g+$, $g+$), 1($g+$, t)
MSGluAgb4	−148.2	25	64	10($g-$, $g+$), 6(t, $g+$)
MSGluAgp3	−140.6	19	47	6(t, $g-$), 2($g+$, $g-$), 1($g+$, $g+$)
MSGluAgp4	−143.1	24	58	6(t, $g+$), 5($g-$, $g+$), 2($g-$, $g-$), 1(t, $g-$)
MSAadAgh3	−158.2	102	100	78($g+$, $g+$), 16($g+$, t), 5($g-$, $g+$), 3(t, $g+$)
MSAadAgh4	−157.3	154	100	75($g-$, $g+$), 52(t, $g+$), 19($g+$, $g+$), 6($g-$, t), 2(t, t)
MSAadArg3	−153.1	81	100	41 ($g+$, $g+$), 25($g+$, t), 12(t, t), 3(t, $g+$)
MSAadArg4	−153.3	100	100	37($g-$, $g+$), 31(t, $g+$), 17($g+$, $g+$), 9(t, t), 6($g-$, t)
MSAadAgb3	−152.6	10	100	10($g+$, $g+$)
MSAadAgb4	−152.5	57	93	24($g-$, $g+$), 22(t, $g+$), 7($g+$, $g+$)
MSAadAgp3	−147.1	10	100	5($g+$, $g-$), 3($g+$, $g+$), 2(t, $g-$)
MSAadAgp4	−147.2	85	74	29(t, $g+$), 16(t, $g-$), 11($g-$, $g-$), 7($g-$, $g+$)

[a] The number of conformations within 4 kcal of the lowest energy conformer for each peptide

[b] The percentage of conformations within 4 kcal of the lowest energy conformer with a Zbb–Xaa salt bridge, which is a hydrogen bonded ion pair (Marqusee and Baldwin 1987)

entropic reasons, consistent with the CD data of the Aad-Xaa peptides at pH 7 (Fig. 2; Tables S1, S2).

The conformations of the low energy conformers that formed intrahelical salt bridges were then inspected in detail (Table 3; Figs. 5, 6). Since none of the model peptides with Zbb–Xaa (i, $i + 5$) sequence patterns formed salt bridges, these model peptides will not be discussed further. The combination of χ_1 dihedrals is represented in parentheses (Tables 3, S3), designating the conformation for the negatively charged residue at position i followed by the conformation for the positively charged residue at position $i + 3$ or $i + 4$. For example, the conformation with t for both residues at positions i and $i + 3$ would be designated (t, t) for (i, $i + 3$).

Low energy conformers with intrahelical salt bridges were observed for all MSZbbXaa3 model peptides (Table 3; Fig. 5). For MSAspXaa3 model peptides, the major dihedral combination for model peptides MSAspAgh3 and MSAspArg3 with an intrahelical salt bridge was ($g+$, $g+$); the minor combination was ($g+$, t) (Table 3; Fig. 5). Furthermore, the low energy conformers for model peptide MSAspAgb3 with intrahelical salt bridges all involved the dihedral combination ($g+$, $g+$) (Table 3; Fig. 5). Interestingly, the dihedral combinations for model peptide MSAspAgp3 with intrahelical salt bridges were (t, $g-$) and ($g+$, $g-$), with (t, $g-$) as the major dihedral combination (Table 3; Fig. 5). For model peptide MSGluAgh3, ($g+$, $g+$) was the only low energy dihedral combination with intrahelical salt bridges. The dihedral combinations for model peptides MSGluArg3 and MSGluAgb3 with intrahelical salt bridges were ($g+$, $g+$) and ($g+$, t), with ($g+$, $g+$) as the major dihedral combination. Furthermore, the major dihedral combination for model peptide MSGluAgp3 with an intrahelical salt bridge was (t, $g-$), with the minor dihedral combinations ($g+$, $g-$) and ($g+$, $g+$). The major low energy dihedral combination for MSAadXaa3 model peptides with an intrahelical salt bridge was ($g+$, $g+$) for the positively charged residues Agh, Arg, and Agb (Table 3; Fig. 5). However, the major low energy dihedral combination for model peptide

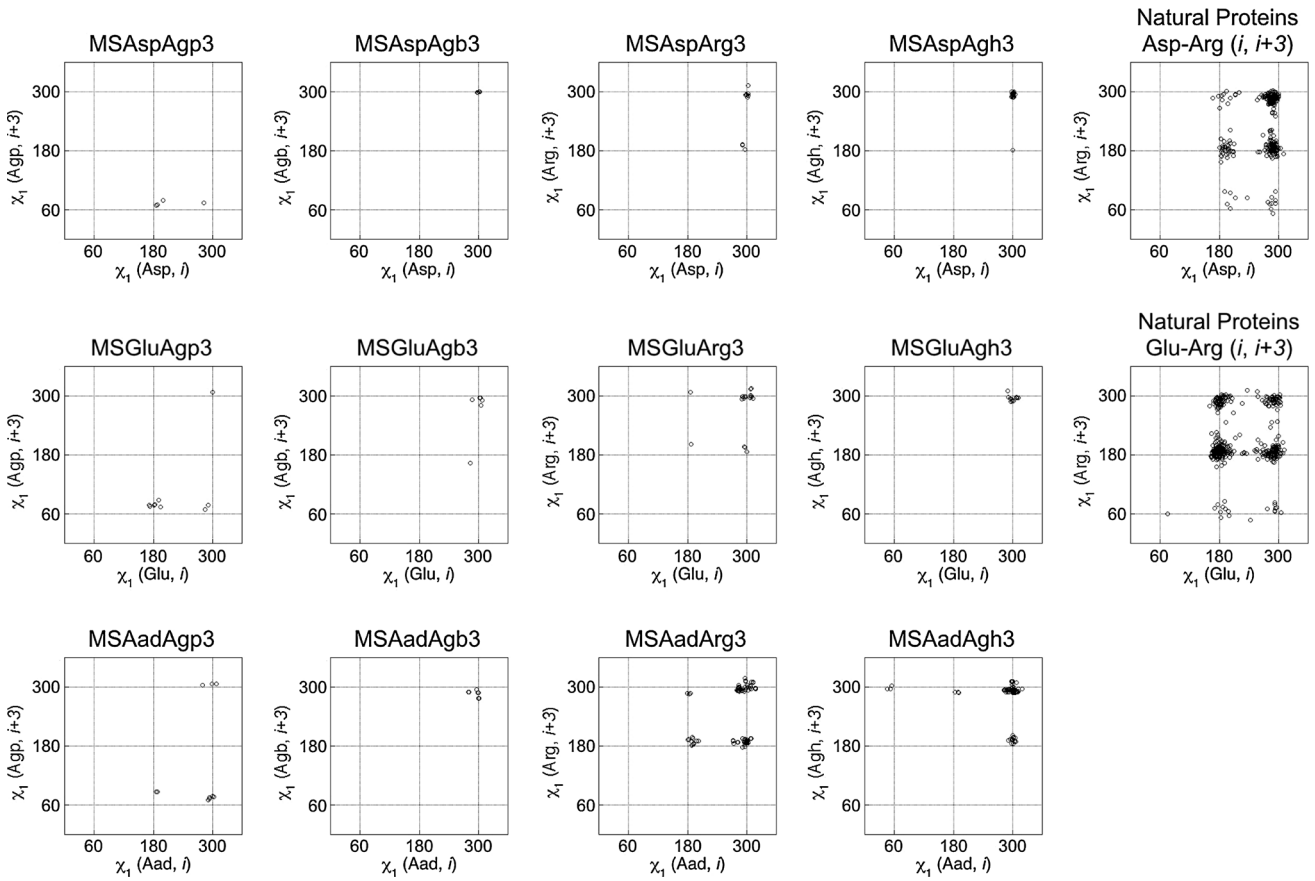

Fig. 5 χ_1 (Zbb, i) − χ_1 (Xaa, $i + 3$) plots for MSZbbXaa3 peptides with salt bridges within 4 kcal of the lowest energy conformation from conformational analysis by molecular mechanics calculations are in the *left four columns* (*top row from left to right*, MSAspAgp3, MSAspAgb3, MSAspArg3, MsAspAgh3; *middle row from left to right*, MSGluAgp3, MSGluAgb3, MSGluArg3, MSGluAgh3; *bottom row from left to right*, MSAadAgp3, MSAadAgb3, MSAadArg3, MSAadAgh3). The side chain conformation of intrahelical Asp–Arg (i, $i + 3$) and Glu–Arg (i, $i + 3$) salt bridges from the survey of natural proteins are in the *most right-hand-side column*

MSAadAgp3 with an intrahelical salt bridge was ($g+$, $g-$) with the minor dihedral combinations ($g+$, $g+$) and (t, $g-$). According to these results, the major low energy dihedral combination for MSZbbXaa3 model peptides except for MSZbbAgp3 was ($g+$, $g+$). Shortening the positively charged residue to Agp maintained intrahelical salt bridges with a different major dihedral combination.

Low energy conformers with intrahelical salt bridges were observed for all MSZbbXaa4 model peptides (Table 3; Fig. 6). The major low energy dihedral combination with intrahelical salt bridges was ($g-$, $g+$) for the model peptides MSZbbAgh4, MSZbbArg4, and MSZbbAgb4, but was (t, $g+$) for the MSZbbAgp4 model peptides (Table 3; Fig. 6). The involvement of ($g-$, $g+$) and (t, $g+$) for model peptides with oppositely charged residues spaced four residues apart was similar to our previous study involving Lys analogs (Cheng et al. 2012a). For model peptide MSAspAgh4, the major low energy dihedral combination was ($g-$, $g+$) (Table 3; Fig. 6), with minor dihedral combinations ($g+$, $g+$) and ($g-$, t). The only low energy dihedral combination for model peptides MSAspArg4 and MSAspAgb4 was ($g-$, $g+$), whereas the only dihedral combination for model peptide MSAspAgp4 was (t, $g+$) (Table 3; Fig. 6). All MSGluXaa4 model peptides exhibited the dihedral combination ($g-$, $g+$) for low energy conformations with salt bridges (Table 3; Fig. 6). Furthermore, the major low energy dihedral combination for model peptides MSGluAgh4, MSGluArg4, and MSGluAgb4 was ($g-$, $g+$). For model peptide MSGluAgp4, both ($g-$, $g+$) and (t, $g+$) were major low energy dihedral combinations. All the MSAadXaa4 model peptides exhibited the dihedral combination ($g-$, $g+$) (Table 3; Fig. 6), similar to the MSGluXaa4 model peptides with salt bridges. However, (t, $g+$) was also present for all MSAadXaa4 model peptides. For model peptides MSAadAgh4, MSAadArg4, and MSAadAgb4, the dihedral combination ($g-$, $g+$) was the major low energy conformer, whereas (t, $g+$) was slightly less significant. In contrast, (t, $g+$) was the major low energy dihedral combination for model peptide MSAadAgp4, whereas ($g-$, $g+$) was much less significant. Model

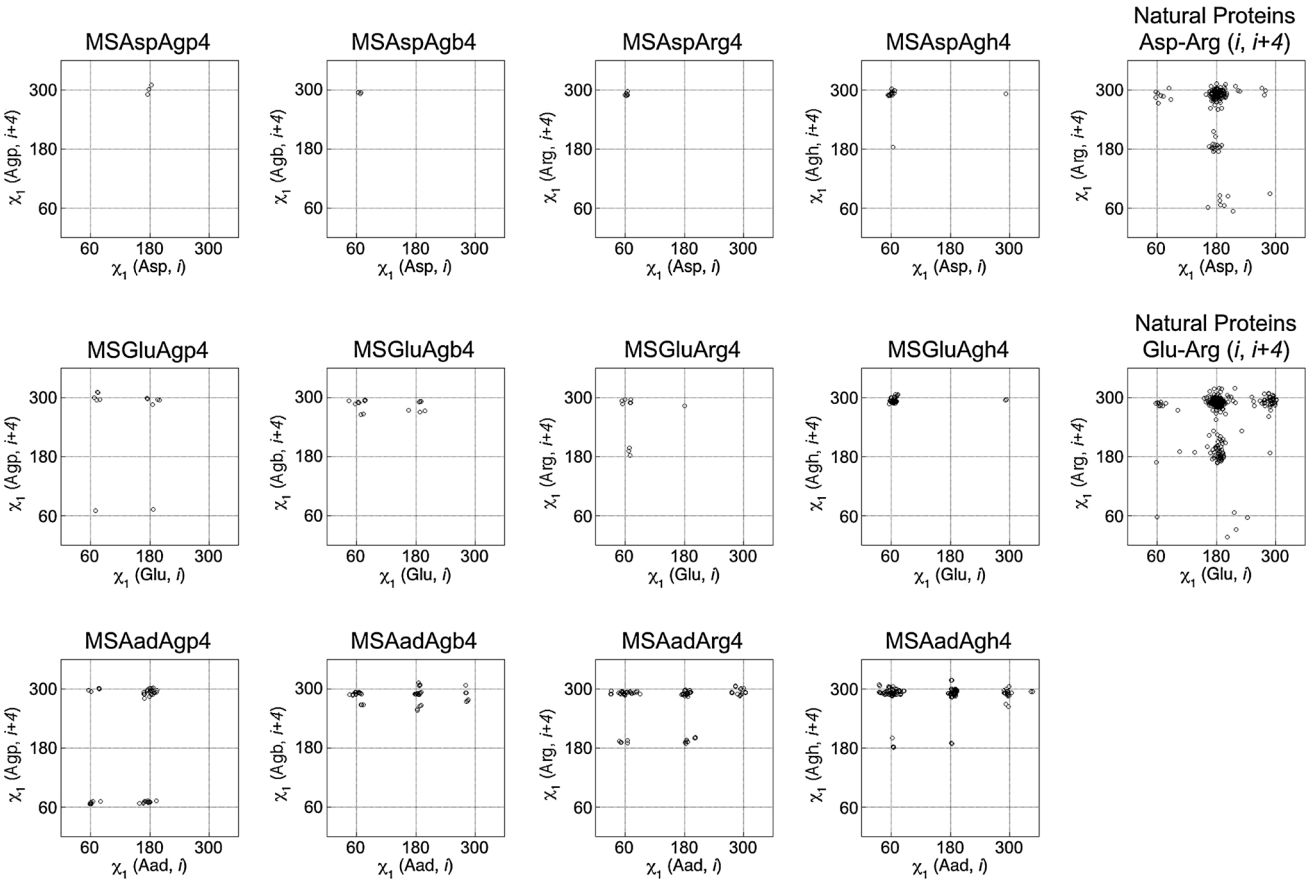

Fig. 6 χ_1(Zbb, i) − χ_1(Xaa, $i + 4$) plots for MSZbbXaa4 peptides with salt bridges within 4 kcal of the lowest energy conformation from conformational analysis by molecular mechanics calculations are in the *left four columns* (*top row from left to right*, MSAspAgp4, MSAspAgb4, MSAspArg4, MSAspAgh4; *middle row from left to right*, MSGluAgp4, MSGluAgb4, MSGluArg4, MSGluAgh4; *bottom row from left to right*, MSAadAgp4, MSAadAgb4, MSAadArg4, MSAadAgh4). The side chain conformation of intrahelical Asp–Arg(i, $i + 4$) and Glu–Arg(i, $i + 4$) salt bridges from the survey of natural proteins are in the *most right-hand-side column*

peptides with the longer side chain residues with salt bridges such as MSAadAgh4, MSAadArg4, MSAadAgb4, MSGluAgh4, and MSAspAgh4 also exhibited the dihedral combination ($g+$, $g+$) (Table 3; Fig. 6). Overall, the major low energy conformation for supporting Zbb–Xaa (i, $i + 4$) salt bridges was similar regardless of side chain length except for peptides containing the shortest positively charged residue Agp.

The molecular mechanics calculation results appeared to be consistent with the experimental data, providing conformational insight for both the encoded and the non-canonical amino acids. The major dihedral combinations to support intrahelical salt bridges were ($g+$, $g+$) and ($g-$, $g+$) for model peptides MSZbbXaa3 and MSZbbXaa4, respectively, except for the Agp-containing model peptides. However, it was unclear whether or not these conformational preferences for the encoded residues were represented in natural protein structures. To further confirm the results from the conformational analysis, intrahelical Asp–Arg and Glu–Arg sequence patterns and salt bridges in natural proteins were examined for comparison.

Intrahelical Asp–Arg and Glu–Arg sequence patterns and salt bridges in protein structures

A survey was performed on the non-redundant protein structure database PDBselect (April 2009, 25 % threshold) (Hobohm and Sander 1994; Griep and Hobohm 2010) to explore the side chain conformations that support intrahelical Asp–Arg and Glu–Arg interactions in naturally occurring proteins (Tables 4, S4, S5). A total of 666,086 residues in 4,418 protein chains were considered. The α-helical conformation was defined based on backbone dihedrals (Gunasekaran et al. 1998; Engel and DeGrado 2004; Cheng et al. 2007, 2010, 2012a, b). Only α-helices of six residues or longer were considered to exclude helices with less than one turn (Cheng et al. 2007, 2010, 2012a, b). Based on these criteria, there were 236,790 helical residues

Table 4 Survey results of oppositely charged residues with various spacings in natural protein helices

Position i	Position $i + n$	n	Occurrence[a]	Helix pair propensity[b]	Pair propensity[c]	Salt bridge occurrence[d]	Major conformations with salt bridge number (Zbb χ_1, Xaa χ_1)
Glu	Arg	3	1,659	2.06 ± 0.07	1.36 ± 0.03	431	194(t, t), 105($g+$, t), 64(t, $g+$), 49($g+$, $g+$)
Asp	Arg	3	869	1.52 ± 0.06	1.38 ± 0.05	247	103($g+$, $g+$), 83($g+$, t), 34(t, t), 12(t, $g+$)
Glu	Arg	4	1,476	2.15 ± 0.08	1.33 ± 0.03	309	194(t, $g+$), 54(t, t), 42($g+$, $g+$), 11($g-$, $g+$)
Asp	Arg	4	733	1.45 ± 0.06	1.27 ± 0.05	157	123(t, $g+$), 15(t, t), 8($g-$, $g+$), 7(t, $g-$)
Glu	Arg	5	778	1.54 ± 0.07	0.78 ± 0.02	1	1(t, $g+$)
Asp	Arg	5	441	0.98 ± 0.05	0.85 ± 0.03	0	

[a] The occurrence of oppositely charged residues placed three, four, and five residues apart in helices six residues or longer in the non-redundant protein structure database PDBselect (April 2009, 25 % threshold) (Hobohm and Sander 1994; Griep and Hobohm 2010). The helix conformation is defined by the backbone dihedral angles (ϕ, ψ) according to the values provided by Balaram and coworkers (Gunasekaran et al. 1998; Engel and DeGrado 2004; Cheng et al. 2007, 2010, 2012a, b)

[b] The occurrence for the various sequence patterns divided by the corresponding expected value. The expected value was obtained by bootstrapping the complete PDBselect database, thereby including the bias for the occurrence of each residue for the helix conformation. Since bootstrapping was performed 100,000 times, this enabled the calculation of a standard deviation for the expected value and thus helix pair propensity

[c] The occurrence for the various sequence patterns divided by the corresponding expected value. The expected value was obtained by bootstrapping the helices in the PDBselect database, thereby removing the bias for the occurrence of each residue for the helix conformation. Since bootstrapping was performed 100,000 times, this enabled the calculation of a standard deviation for the expected value and thus helix pair propensity

[d] The number of the occurrences for each sequence pattern that actually forms salt bridges between the oppositely charged side chain functionalities. The presence of a salt bridge is defined by an N–O distance $\leq$3 Å

in 17,622 helices. The number of occurrences for Asp–Arg and Glu–Arg sequence patterns with (i, $i + 3$), (i, $i + 4$), and (i, $i + 5$) spacings were compiled (Table 4). Helix pair propensity represents how frequently a particular sequence pattern occurs in a helix compared to any structure in the database. This would include contributions from both how frequently the amino acids in the sequence pattern occur in helices, and how frequently the sequence pattern itself occurs in the context of a helix. In contrast, pair propensity in a helix represents how frequently a sequence pattern occurs in the context of a helix. The propensity for each sequence pattern was derived by dividing the occurrence by the expected occurrence in the appropriate context. The expected occurrence was obtained by bootstrapping the entire database for the helix pair propensity, and by bootstrapping the helical residues in the database for the pair propensity (in helices). Helix pair propensities greater than unity represent higher occurrence compared to expected occurrence in all structures, whereas pair propensities greater than unity indicate higher occurrence compared to expected occurrence in helices in the database. As such, helix pair propensities less than unity represent lower occurrence compared to the expected value for all structures, whereas pair propensities less than unity indicate lower occurrence compared to the expected value for helical structures.

The helix pair propensity for both Asp–Arg and Glu–Arg (i, $i + n$) sequence patterns followed the trend (i, $i + 3$) $\sim$ (i, $i + 4$) $>$ (i, $i + 5$) (Tables 4, S4). Furthermore, the helix pair propensity for sequence patterns involving Glu was higher than that for the corresponding patterns involving Asp. However, the helix pair propensity for a given sequence pattern is determined by both the inherent frequency of occurrence of the amino acid in a helix and the prevalence of the sequence pattern in a helix (i. e., the pair propensity in helix). To remove the bias caused by the inherent frequency of occurrence for the amino acids in a helix, the pair propensity for each sequence pattern was also derived (Tables 4, S5). Sequence patterns with (i, $i + 3$) and (i, $i + 4$) spacings exhibited pair propensities greater than unity, whereas sequence patterns with (i, $i + 5$) spacing exhibited pair propensities lower than unity.

The three-dimensional structures of these occurrences with salt bridges were then examined in detail. Salt bridges were defined by an N–O distance of 3 Å or less. Only a small portion of the sequence patterns were manifested as salt bridge interactions in the protein structure (Table 4), similar to findings by Thornton and coworkers (Barlow and Thornton 1983). Furthermore, Asp–Arg and Glu–Arg (i, $i + 5$) salt bridges were essentially non-existent (Table 4). The side chain conformations of the intrahelical Asp/Glu–Arg (i, $i + 3$) and (i, $i + 4$) salt bridges were then examined further (Table 4; last column in Figs. 5, 6). The most prevalent χ_1 dihedral combinations for both Asp–Arg and Glu–Arg (i, $i + 3$) intrahelical salt bridges were ($g+$, $g+$), ($g+$, t), (t, t), and (t, $g+$), which includes the major dihedral combination ($g+$, $g+$) from the conformational analysis by

molecular mechanics calculations (Table 3; Fig. 5). The major χ_1 dihedral combinations for both Asp–Arg and Glu–Arg (i, $i + 4$) intrahelical salt bridges were (t, $g+$), (t, t), and ($g-$, $g+$), which also includes the major dihedral combination ($g-$, $g+$) from the conformational analysis by molecular mechanics calculations (Table 3; Fig. 6). Importantly, the combinations of χ_1 dihedrals for the Asp–Arg and Glu–Arg intrahelical salt bridges in natural protein structures included those from the molecular mechanics calculations (Figs. 5, 6), validating the conformational analysis results.

Discussion

A series of helical peptides containing guanidinium- and carboxylate-bearing amino acids were investigated to gain insight into how altering the side chain length of the charged residues Arg and Glu/Asp affects intrahelical interactions and helicity. The helical content of the peptides was determined by CD spectroscopy at pH 7 and pH 2. As the pH was changed from 7 to 2, the negatively charged Zbb^- would be protonated and neutralized to Zbb^0. Accordingly, changes in the CD signal should reflect changes in both electrostatic interactions (between Zbb^- and Xaa, and between Zbb^- and the helix macrodipole) and helix propensity. Interestingly, the helical content of most of the Glu-containing and Aad-containing peptides did not alter significantly with pH (Fig. 3). The lack of significant change in the CD signal for these peptides suggests that the effects most likely cancel one another. In contrast, the helical content for most of the Asp-containing peptides was significantly attenuated upon changing the pH from 7 to 2, suggesting that the loss of favorable electrostatic interactions involving Zbb^- outweighed the minimal change or only slight increase in helix propensity for Asp (Huyghues-Despointes et al. 1993a; Chakrabartty et al. 1994; Kobayashi et al. 1977). Based on how peptide helicity depends on the pH, Asp is clearly different from Glu, whereas Glu and Aad are similar.

The ZbbXaa5 peptides should not exhibit any intrahelical interaction between the charged residues spaced five residues apart, based on the helix geometry. This was the case for the GluXaa5 and AadXaa5 peptides (Table S2). However, the AspXaa5 peptides appeared to exhibit intrahelical interaction energy at pH 7 (Tables 2, S2). Based on the difference between the interaction energy at pH 7 and 2, electrostatics dominated the apparent interaction energy at pH 7 for AspXaa5 peptides (Tables 2, S2). Furthermore, AspAgb5 and AspArg5 showed weaker interaction energies at pH 2 compared to pH 7. Importantly, none of the MSAspXaa5 model peptides exhibited intrahelical Asp–Xaa salt bridges in the conformational analysis by molecular mechanics calculations (Table S3). As such, the apparent interaction energies for the AspXaa5 peptides were most likely Xaa–Asp (i, $i + 1$) interactions opposed to Asp–Xaa (i, $i + 5$) interactions. Overall, this suggested that electrostatics was an important component of the potential Xaa–Asp^- (i, $i + 1$) interactions to stabilize the helical conformation at pH 7. Furthermore, the electrostatic contribution of the Xaa–Asp^- (i, $i + 1$) interaction energy at pH 7 followed the trend Agp > Agb > Arg > Agh, apparently decreasing with increasing Xaa side chain length.

The helical content for ZbbArg3 peptides at pH 7 followed the trend AadArg3 > GluArg3 > AspArg3 (Fig. 2; Table S1), consistent with the results on analogous Asp/Glu–Arg peptides reported by Baldwin (Huyghues-Despointes et al. 1993b). For ZbbXaa3 peptides at pH 7, Arg supported significant helicity with any negatively charged residue, whereas both Agh and Agb were capable of supporting intermediate and significant helicity with Glu and Aad, respectively (Fig. 2; Table S1). This was different from the Lys analogs (Cheng et al. 2012a), in which only Lys-containing peptides with potential Zbb–Lys (i, $i + 3$) interactions exhibited significant helicity at pH 7 (Cheng et al. 2012a). This may be caused by the more diffuse positive charge for the guanidinium group (on Agb, Arg, and Agh) compared to the ammonium group (on Lys), the different shape of the functional groups, or the varying overall length of the residues; Agb has the same overall length as Lys, whereas Arg and Agh are both longer than Lys. Accordingly, Zbb–Xaa (i, $i + 3$) interactions were affected by not only the length of side chain but also the charge distribution on the functional group. For peptides AspArg3 and GluArg3, the magnitude of the CD signal at pH 7 was noticeably higher than that at pH 2 (Fig. 3a, d; Table S1). This was similar to the results reported by Baldwin (Huyghues-Despointes et al. 1993b), and mirrors earlier results on peptides with intrahelical Asp–Lys and Glu–Lys (i, $i + 3$) ion pairing interactions (Cheng et al. 2012a). Furthermore, among the three Arg-containing peptides with significant helicity (AspArg3, GluArg3, and AadArg3), only AspArg3 exhibited a stabilizing Zbb^-–Arg (i, $i + 3$) interaction energy. Increasing the negatively charged Asp side chain length resulted in essentially no Glu^-–Xaa (i, $i + 3$) and Aad^-–Xaa (i, $i + 3$) interactions. This may be due to the increased entropic penalty, or the need to adopt higher energy conformations to form intrahelical salt bridges for the longer Aad and Glu side chains compared to the shorter Asp side chain. Nonetheless, the Asp–Agh/Arg/Agb (i, $i + 3$) interactions were completely electrostatics according to the interaction energy at the different pH values (Tables 2, S2).

The helical content of ZbbXaa4 peptides was higher compared to the helical content of the corresponding

ZbbXaa3 peptides (Figs. 2, 3; Table S1), similar to the Lys analog-containing peptides (Cheng et al. 2012a). Furthermore, this experimental observation was generally consistent with the conformational analysis results, in which the MSAspXaa4 and MSGluXaa4 model peptides were lower in energy (i.e., more stable) compared to the corresponding MSAspXaa3 and MSGluXaa3 model peptides (Tables 3, S3), respectively. The largest energy difference was observed between model peptides MSAspAgb4 and MSAspAgb3 (Table 3), consistent with the high helical content for peptide AspAgb4 with high stabilizing side chain interaction (Fig. 2; Tables 1, S1, S2), and the low helical content for peptide AspAgb3 with minimal side chain interactions (Fig. 2; Tables 2, S1, S2). Similarly, a large energy difference was also observed between model peptides MSAspAgp4 and MSAspAgp3 (Table 3), consistent with the high helical content for peptide AspAgp4 and low helical content for peptide AspAgp3 (Fig. 2; Table S1). In contrast, model peptides MSAadXaa4 and MSAadXaa3 were similar in energy. However, the MSAadXaa4 model peptides exhibited more low energy conformers compared to MSAadXaa3 model peptides (Table 3), suggesting that the Aad–Xaa (i, $i + 4$) interactions were entropically more favorable compared to the Aad–Xaa (i, $i + 3$) interactions.

The helical content for AspArg4 was less than that for GluArg4 at both pH values 7 and 2 (Figs. 2, 3; Table S1), similar to the results reported by Baldwin (Huyghues-Despointes et al. 1993b). The Zbb^{-}–Xaa (i, $i + 4$) interactions at pH 7 became more stabilizing as the positively or negatively charged residues side chain length decreased for ZbbXaa4 peptides with significant helical content (i.e., AspAgh4, AspArg4, AspAgb4; AadArg4, AadAgb4, AadAgp4; GluAgh4, GluArg4, GluAgb4) (Tables 1, S2). Interestingly, the helical content of peptide AspArg4 was much higher compared to AspAgh4, despite having similar Asp^{-}–Xaa (i, $i + 4$) interaction energies. Also, the Glu^{-}–Agb, Glu^{-}–Arg, and Glu^{-}–Agh (i, $i + 4$) interactions were energetically similar, but the helical content of peptide GluArg4 was much higher compared to peptides GluAgb4 and GluAgh4. These apparent discrepancies are due to the difference in helix propensity for the guanidinium-containing residues Agb, Arg, and Agh (Cheng et al. 2012b). Apparently, the side chain length of the positively charged amino acids Xaa may be for reaching to enable favorable Zbb–Xaa (i, $i + 4$) interactions. Side chains too short to reach, such as that of Agp, did not seem to support Glu/Asp–Agp (i, $i + 4$) interactions. Only Aad has a side chain long enough to reach and interact with Agp to form stabilizing Aad–Agp (i, $i + 4$) interactions (Tables 1, S2). Furthermore, the Aad^{-}–Agp (i, $i + 4$) interaction at pH 7 was completely electrostatics based on pH-dependent studies (Tables 1, S2). However, the side chain combinations in peptides AadAgh4 and AadArg4 did not support stabilizing Zbb–Xaa (i, $i + 4$) interactions. This may be because the longer side chain is more flexible, increasing the entropic penalty upon forming an ion pair, resulting in the non-existent interaction energy. Another possibility is the combination of the longer residues results in Xaa–Zbb (i, $i + 1$) interactions that stabilize non-helical conformations (Scholtz et al. 1993).

The helical content of all AspXaa4 peptides decreased upon lowering the pH from 7 to 2 (Fig. 3b; Table S1). This is most likely due to the loss of Asp^{-}–Xaa (i, $i + 4$) electrostatic interactions, the loss of favorable Asp^{-}–helix dipole interactions, and minimal change or only slight increase in helix propensity of Asp^{-} upon protonation to Asp^{0} (Huyghues-Despointes et al. 1993a; Chakrabartty et al. 1994; Kobayashi et al. 1977). This pH dependence for Asp-containing peptides with Arg analogs is similar to the Asp-containing peptides with Lys analogs (Cheng et al. 2012a; Huyghues-Despointes et al. 1993a; Chakrabartty et al. 1994; Doig and Baldwin 1995). The side chain length of Arg could be shortened or lengthened by one methylene (to Agb and Agh) to enhance the Asp–Xaa (i, $i + 4$) electrostatics in both AspAgb4 and AspAgh4 peptides (Tables 1, S2). Interestingly, the Asp^{-}–Agh (i, $i + 4$) interaction at pH 7 was completely electrostatics based on pH dependence data (Tables 1, S2). The Asp–Arg (i, $i + 4$) interaction was predominantly electrostatics at pH 7, whereas the electrostatic component for the Asp–Agb (i, $i + 4$) interaction at pH 7 was significant but not dominating (Tables 1, S2). The presence of Asp^{0}–Agb and Asp^{0}–Arg (i, $i + 4$) interactions at pH 2 suggested that the Asp^{-}–Agb and Asp^{-}–Arg (i, $i + 4$) interactions at pH 7 included non-electrostatic components such as hydrogen bonding (Huyghues-Despointes et al. 1993a; Marqusee and Baldwin 1987) or hydrophobics (Cheng et al. 2007; Andrew et al. 2001). The side chain–side chain hydrogen bond would bring the two functionalities into close proximity, whereas the hydrophobic methylenes on the side chains would shield the helix hydrogen bonds to stabilize the helix conformation (Groebke et al. 1996; Luo and Baldwin 1999; Garcia and Sanbonmatsu 2002).

The Glu–Arg (i, $i + 4$) interaction was predominantly electrostatics based on the pH dependence results (Tables 1, S2). Shortening or lengthening the side chain length of Arg by one methylene (to Agb and Agh) reduced the electrostatic component in both Glu–Agb and Glu–Agh (i, $i + 4$) interactions (Tables 1, S2). Furthermore, the Glu–Agb (i, $i + 4$) and Glu–Agh (i, $i + 4$) interactions were not predominantly electrostatics. The significant Glu^{0}–Agb and Glu^{0}–Agh (i, $i + 4$) interactions at pH 2 may be also due to side chain–side chain hydrogen bonding[30, 64] or hydrophobics (Andrew et al. 2001).

The helix pair propensity for both Asp–Arg and Glu–Arg (i, $i + n$) sequence patterns followed the trend (i, $i + 3$) ~ (i, $i + 4$) > (i, $i + 5$) (Tables 4, S4). These results were different from the Asp–Lys and Glu–Lys helix pair propensity trend (i, $i + 4$) > (i, $i + 3$) > (i, $i + 5$) (Cheng et al. 2012a). This suggests that Arg and Lys are applied differently in natural protein helices with different spacings. The Asp–Arg and Glu–Arg sequence patterns with (i, $i + 3$) and (i, $i + 4$) spacings occur more frequently than expected in helical structures, but Asp–Arg and Glu–Arg (i, $i + 5$) do not occur as frequently as expected. These results were the same as those for the intrahelical Asp–Lys and Glu–Lys sequence patterns (Cheng et al. 2012a).

Conclusion

The effect of varying the side chain length on side chain interactions between carboxylate- and guanidinium-bearing residues in an α-helix has been studied by CD. The Arg-containing peptides consistently showed higher helicity compared to the corresponding Agp-, Agb-, and Agh-containing peptides. Furthermore, the helicity of the Asp-containing peptides showed significant pH dependence, whereas the Glu- and Aad-containing peptides mostly did not. Apparently, the shorter Asp is distinctly different from the two longer negatively charged residues Glu and Aad. The Zbb–Xaa (i, $i + 4$) interaction becomes more stabilizing upon shortening the side chain length of the carboxylate-containing amino acids, and upon shortening the side chain length of the guanidinium-containing amino acids. The helical content trends of the peptides were recapitulated in the conformational analysis by molecular mechanics calculations (Table 3). On the basis of these calculations, the low energy dihedral combinations for Zbb–Arg analogs (i, $i + 3$) and (i, $i + 4$) were ($g+$, $g+$) and (t, $g+$), respectively. The same conformations were observed in a survey on natural protein helices involving intrahelical Asp–Arg and Glu–Arg salt bridges. Importantly, nature may have chosen Arg to form stable helices. Furthermore, helices with intrahelical Asp–Arg ion pairs would exhibit pH dependence, whereas helices with intrahelical Glu–Arg ion pairs would be invariant to pH changes. These results should be useful in designing structures with robust helices over a wide pH range for peptide-based materials (Pepe-Mooney and Fairman 2009; Lu et al. 2011), and helix-based pH-dependent peptide switches (Altman et al. 2000; Hong et al. 2003; Kuehne and Murphy 2001; Haas and Murphy 2004a, b; Turk et al. 2002; Zimenkov et al. 2006; Sheparovych et al. 2009; Hirosue and Weber 2006; Pagel and Koksch 2008).

Acknowledgments This work was supported by National Taiwan University (NTU-ERP-103R891302) and the Ministry of Science and Technology in Taiwan (former National Science Council; NSC-97-2113-111-002-019-MY2, NSC-98-2119-M-002-025, NSC-99-2113-M-002-002-MY2, NSC-101-2113-M-002-006-MY2). The authors would like to thank the Computer and Information Networking Center at National Taiwan University for the support of the high-performance computing facilities.

Conflict of interest The authors declare that they have no conflict of interest.

References

Altman M, Lee P, Rich A, Zhang S (2000) Conformational behavior of ionic self-complementary peptides. Protein Sci 9(6):1095–1105

Andrew CD, Penel S, Jones GR, Doig AJ (2001) Stabilizing nonpolar/polar side-chain interactions in the α-helix. Proteins Struct Funct Genet 45(4):449–455

Anfinsen CB (1973) Principles that govern folding of protein chains. Science 181(4096):223–230. doi:10.1126/Science.181.4096.223

Atherton E, Fox H, Harkiss D, Logan CJ, Sheppard RC, Williams BJ (1978) Mild procedure for solid phase peptide synthesis—use of fluorenylmethoxycarbonylamino-acids. J Chem Soc Chem Commun 13:537–539. doi:10.1039/C39780000537

Baldwin RL, Rose GD (1999a) Is protein folding hierarchic? I. Local structure and peptide folding. Trends Biochem Sci 24(1):26–33. doi:10.1016/S0968-0004(98)01346-2

Baldwin RL, Rose GD (1999b) Is protein folding hierarchic? II. Folding intermediates and transition states. Trends Biochem Sci 24(2):77–83. doi:10.1016/S0968-0004(98)01345-0

Barlow DJ, Thornton JM (1983) Ion-pairs in proteins. J Mol Biol 168(4):867–885

Chakrabartty A, Kortemme T, Padmanabhan S, Baldwin RL (1993) Aromatic side-chain contribution to far-ultraviolet circular-dichroism of helical peptides and its effect on measurement of helix propensities. Biochemistry 32(21):5560–5565. doi:10.1021/Bi00072a010

Chakrabartty A, Kortemme T, Baldwin RL (1994) Helix propensities of the amino acids measured in alanine-based peptides without helix-stabilizing side-chain interactions. Protein Sci 3(5):843–852. doi:10.1002/pro.5560030514

Chang CT, Wu C-SC, Yang JT (1978) Circular dichroic analysis of protein conformation: inclusion of the β-turns. Anal Biochem 91(1):13–31. doi:10.1016/0003-2697(78)90812-6

Cheng RP, Girinath P, Ahmad R (2007) Effect of lysine side chain length on intra-helical glutamate-lysine ion pairing interactions. Biochemistry 46:10528–10537

Cheng RP, Girinath P, Suzuki Y, Kuo H-T, Hsu H-C, Wang W-R, Yang P-A, Gullickson D, Wu C-H, Koyack MJ, Chiu H-P, Weng Y-J, Hart P, Kokona B, Fairman R, Lin T-E, Barrett O (2010) Positional effects on helical Ala-based peptides. Biochemistry 49:9372–9384

Cheng RP, Wang W-R, Girinath P, Yang P-A, Ahmad R, Li J-H, Hart P, Kokona B, Fairman R, Kilpatrick C, Argiros A (2012a) Effect of glutamate side chain length on intrahelical glutamate-lysine ion pairing interactions. Biochemistry 51(36):7157–7172. doi:10.1021/bi300655z

Cheng RP, Weng Y-J, Wang W-R, Koyack MJ, Suzuki Y, Wu C-H, Yang PA, Hsu H-C, Kuo H-T, Girinath P, Fang C-J (2012b) Helix formation and capping energetics of arginine analogs with varying side chain length. Amino Acids 43(1):195–206. doi:10.1007/s00726-011-1064-2

Creighton TE (1993) Proteins, structure and molecular properties, 2nd edn. W. H. Freeman and Co., New York
Dill KA (1990) Dominant forces in protein folding. Biochemistry 29(31):7133–7155
Dill KA, Ozkan SB, Shell MS, Weikl TR (2008) The protein folding problem. Annu Rev Biophys 37:289–316. doi:10.1146/Annurev.Biophys.37.092707.153558
Doig AJ, Baldwin RL (1995) N- and C-capping preferences for all 20 amino acids in α-helical peptides. Protein Sci 4(7):1325–1336. doi:10.1002/pro.5560040708
Dominy BN, Minoux H, Brooks CL (2004) An electrostatic basis for the stability of thermophilic proteins. Proteins 57(1):128–141. doi:10.1002/Prot.20190
Donald JE, Kulp DW, DeGrado WF (2011) Salt bridges: geometrically specific, designable interactions. Proteins 79(3):898–915. doi:10.1002/Prot.22927
Dunbrack RL, Karplus M (1993) Backbone-dependent rotamer library for proteins—application to side-chain prediction. J Mol Biol 230(2):543–574
Edelhoch H (1967) Spectroscopic determination of tryptophan and tyrosine in proteins. Biochemistry 6(7):1948–1954
Elcock AH (1998) The stability of salt bridges at high temperatures: implications for hyperthermophilic proteins. J Mol Biol 284(2):489–502. doi:10.1006/Jmbi.1998.2159
Engel DE, DeGrado WF (2004) Amino acid propensities are position-dependent throughout the length of α-helices. J Mol Biol 337:1195–1205
Fersht AR (1999) Structure and mechanism in protein science. A guide to enzyme catalysis and protein folding. W.H. Freeman and Co., New York
Fields GB, Noble RL (1990) Solid phase peptide synthesis utilizing 9-fluorenylmethoxycarbonyl amino acids. Int J Pept Protein Res 35(3):161–214
Garcia AE, Sanbonmatsu KY (2002) α-Helical stabilization by side chain shielding of backbone hydrogen bonds. Proc Natl Acad Sci USA 99(5):2782–2787. doi:10.1073/Pnas.042496899
Griep S, Hobohm U (2010) PDBselect 1992–2009 and PDBfilter-select. Nucleic Acids Res 38:D318–D319
Groebke K, Renold P, Tsang KY, Allen TJ, McClure KF, Kemp DS (1996) Template-nucleated alanine-lysine helices are stabilized by position-dependent interactions between the lysine side chain and the helix barrel. Proc Natl Acad Sci USA 93(9):4025–4029. doi:10.1073/Pnas.93.9.4025
Gunasekaran K, Nagarajaram HA, Ramakrishnan C, Balaram P (1998) Stereochemical punctuation marks in protein structures: glycine and proline containing helix stop signals. J Mol Biol 275(5):917–932
Haas DH, Murphy RM (2004a) Design of a pH-sensitive pore-forming peptide with improved performance. J Pept Res 63(1):9–16
Haas DH, Murphy RM (2004b) Templated assembly of the pH-sensitive membrane-lytic peptide GALA. J Pept Res 63(6):451–459
Hirosue S, Weber T (2006) pH-dependent lytic peptides discovered by phage display. Biochemistry 45(20):6476–6487
Hobohm U, Sander C (1994) Enlarged representative set of protein structures. Protein Sci 3(3):522–524. doi:10.1002/pro.5560030317
Hong YS, Legge RL, Zhang S, Chen P (2003) Effect of amino acid sequence and pH on nanofiber formation of self-assembling peptides EAK16-II and EAK16-IV. Biomacromolecules 4(5):1433–1442
Huyghues-Despointes BM, Scholtz JM, Baldwin RL (1993a) Effect of a single aspartate on helix stability at different positions in a neutral alanine-based peptide. Protein Sci 2(10):1604–1611
Huyghues-Despointes BM, Scholtz JM, Baldwin RL (1993b) Helical peptides with three pairs of Asp–Arg and Glu–Arg residues in different orientations and spacings. Protein Sci 2(1):80–85. doi:10.1002/pro.5560020108
Jiang YL, Ichikawa Y, Song F, Stivers JT (2003) Powering DNA repair through substrate electrostatic interactions. Biochemistry 42(7):1922–1929. doi:10.1021/bi027014x
Johnsson K, Allemann RK, Widmer H, Benner SA (1993) Synthesis, structure and activity of artificial, rationally designed catalytic polypeptides. Nature 365(6446):530–532
Karshikoff A, Ladenstein R (2001) Ion pairs and the thermotolerance of proteins from hyperthermophiles: a 'traffic rule' for hot roads. Trends Biochem Sci 26(9):550–556. doi:10.1016/S0968-0004(01)01918-1
Klingler TM, Brutlag DL (1994) Discovering structural correlations in α-helices. Protein Sci 3(10):1847–1857. doi:10.1002/pro.5560031024
Kobayashi Y, Cardinaux F, Zweifel BO, Scheraga HA (1977) Helix-coil stability constants for the naturally occurring amino acids in water. 16. Aspartic acid parameters from random poly(hydroxybutylglutamine-*co*-L-aspartic acid). Macromolecules 10:1271–1283
Kuehne J, Murphy RM (2001) Synthesis and characterization of membrane-active GALA-OKT9 conjugates. Bioconjugate Chem 12(5):742–749
Kumar S, Nussinov R (2002) Close-range electrostatic interactions in proteins. ChemBioChem 3(7):604–617. doi:10.1002/1439-7633(20020703)3:7<604:Aid-Cbic604>3.0.Co;2-X
Kuo L-H, Li J-H, Kuo H-T, Hung C-Y, Tsai H-Y, Chiu W-C, Wu C-H, Wang W-R, Yang P-A, Yao Y-C, Wong TW, Huang S-J, Huang S-L, Cheng RP (2013) Effect of charged amino acid side chain length at non-hydrogen bonded strand positions on β-hairpin stability. Biochemistry 52:7785–7797
Lifson S, Roig A (1961) The theory of helix-coil transition in polypeptides. J Chem Phys 34:1963–1974
Lu H, Wang J, Bai Y, Lang JW, Liu S, Lin Y, Cheng J (2011) Ionic polypeptides with unusual helical stability. Nat Commun 2:206
Luo PZ, Baldwin RL (1999) Interaction between water and polar groups of the helix backbone: an important determinant of helix propensities. Proc Natl Acad Sci USA 96(9):4930–4935. doi:10.1073/Pnas.96.9.4930
Makhatadze GI, Privalov PL (1995) Energetics of protein structure. Adv Protein Chem 47:307–425
Malakauskas SM, Mayo SL (1998) Design, structure and stability of a hyperthermophilic protein variant. Nat Struct Biol 5(6):470–475. doi:10.1038/Nsb0698-470
Marqusee S, Baldwin RL (1987) Helix stabilization by Glu-…Lys+ salt bridges in short peptides of de novo design. Proc Natl Acad Sci USA 84(24):8898–8902
Maxfield FR, Scheraga HA (1975) The effect of neighboring charges on the helix forming ability of charged amino acids in proteins. Macromolecules 8(4):491–493
McGregor MJ, Islam SA, Sternberg MJE (1987) Analysis of the relationship between side-chain conformation and secondary structure in globular-proteins. J Mol Biol 198(2):295–310
Pace CN, Scholtz JM (1998) A helix propensity scale based on experimental studies of peptides and proteins. Biophys J 75(1):422–427
Pace CN (2000) Single surface stabilizer. Nat Struct Biol 7(5):345–346. doi:10.1038/75100
Pace CN, Vajdos F, Fee L, Grimsley G, Gray T (1995) How to measure and predict the molar absorption-coefficient of a protein. Protein Sci 4(11):2411–2423
Pace CN, Shirley BA, McNutt M, Gajiwala K (1996) Forces contributing to the conformational stability of proteins. FASEB J 10(1):75–83
Padmanabhan S, York EJ, Stewart JM, Baldwin RL (1996) Helix propensities of basic amino acids increase with the length of the

side-chain. J Mol Biol 257(3):726–734. doi:10.1006/jmbi.1996.0197

Pagel K, Koksch B (2008) Following polypeptide folding and assembly with conformational switches. Curr Opin Chem Biol 12:730–739

Pauling L, Corey RB, Branson HR (1951) The structure of proteins; two hydrogen-bonded helical configurations of the polypeptide chain. Proc Natl Acad Sci USA 37(4):205–211

Pepe-Mooney BJ, Fairman R (2009) Peptides as materials. Curr Opin Struct Biol 19:483–494

Robert CH (1990) A hierarchical nesting approach to describe the stability of α-helices with side-chain interactions. Biopolymers 30(3–4):335–347

Robinson-Rechavi M, Alibés A, Godzik A (2006) Contribution of electrostatic interactions, compactness and quaternary structure to protein thermostability: lessons from structural genomics of *Thermotoga* maritima. J Mol Biol 356(2):547–557. doi:10.1016/J.Jmb.11.065

Rose GD, Fleming PJ, Banavar JR, Maritan A (2006) A backbone-based theory of protein folding. Proc Natl Acad Sci USA 103(45):16623–16633. doi:10.1073/Pnas.0606843103

Sali D, Bycroft M, Fersht AR (1988) Stabilization of protein-structure by interaction of α-helix dipole with a charged side-chain. Nature 335(6192):740–743

Scholtz JM, Qian H, Robbins VH, Baldwin RL (1993) The energetics of ion-pair and hydrogen-bonding interactions in a helical peptide. Biochemistry 32(37):9668–9676

Sheparovych R, Roiter Y, Yang J, Kopecek J, Minko S (2009) Stimuli-responsive properties of peptide-based copolymers studied via directional growth of self-assembled patterns on solid substrate. Biomacromolecules 10:1955–1961

Smith JS, Scholtz JM (1998) Energetics of polar side-chain interactions in helical peptides: salt effects on ion pairs and hydrogen bonds. Biochemistry 37(1):33–40. doi:10.1021/bi972026h

Su JG, Chen WZ, Wang CX (2010) Role of electrostatic interactions for the stability and folding behavior of cold shock protein. Proteins 78(9):2157–2169. doi:10.1002/Prot.22730

Thomas AS, Elcock AH (2004) Molecular simulations suggest protein salt bridges are uniquely suited to life at high temperatures. J Am Chem Soc 126(7):2208–2214. doi:10.1021/Ja039159c

Turk MJ, Reddy JA, Chmielewski JA, Low PS (2002) Characterization of a novel pH-sensitive peptide that enhances drug release from folate-targeted liposomes at endosomal pHs. Biochim Biophys Acta-Biomembr 1559(1):56–68

Xiao L, Honig B (1999) Electrostatic contributions to the stability of hyperthermophilic proteins. J Mol Biol 289(5):1435–1444. doi:10.1006/Jmbi.1999.2810

Yip KS, Britton KL, Stillman TJ, Lebbink J, De Vos WM, Robb FT, Vetriani C, Maeder D, Rice DW (1998) Insights into the molecular basis of thermal stability from the analysis of ion-pair networks in the Glutamate Dehydrogenase family. Eur J Biochem 255(2):336–346. doi:10.1046/J.1432-1327.1998.2550336.X

Zimenkov Y, Dublin SN, Ni R, Tu RS, Breedveld V, Apkarian RP, Conticello VP (2006) Rational design of a reversible pH-responsive switch for peptide self-assembly. J Am Chem Soc 128:6770–6771